Int. J. Electrochem. Sci., 10 **(2015)** 2281 - 2290

International Journal of
ELECTROCHEMICAL
SCIENCE
www.electrochemsci.org

Study on the Electrodeposition of Lead with In-Situ Ellipsometry

Xiaolei Ren, Shengtao Zhang[*]*, Lei Guo, Wenpo Li, Jinglei Lei, Yanru Wang*

School of Chemistry and Chemical Engineering, Chongqing University, Chongqing 400044, P.R. China
[*]E-mail: stzhcq@163.com

Received: 10 December 2014 / *Accepted:* 4 January 2015 / *Published:* 19 January 2015

In this study, we applied the in situ spectroscopic ellipsometry (SE) technology to the electrochemical test, and combined with cyclic voltammetry (CV) mainly researched underpotential-deposited (UPD) of Pb on polycrystalline Cu. The results showed the kinetics of UPD Pb on polycrytalline Cu was a quasi-reversible two dimensional nucleation and growth process, the reversible Pb UPD potential is −350mV. The substrate solution interface structure was described with an effective medium approximation (EMA) model, and the volume fraction of Pb and solution were fitted. Fitting results showed that double layer charge and hydrogen reduction reaction cannot be ignored.

Keywords: Electrodeposition, Lead, Cyclic voltammetry, Spectroscopic ellipsometry

1. INTRODUCTION

Lead electrodeposition has been subject of interest in the past due to its extensive application in the relevant fields. For example, purity lead was widely used in lead-acid battery [1]. High purity active lead was applied in the production of semiconductors [2, 3] and the fabrication of electro-chromic devices [4-6]. The researches of lead electrodeposition focused on the preparation of high quality electrode materials [7-10] as well as composite metallic materials [11, 12] having specific functions.

Although amount of works has been done on the electrodeposition of Pb, there has been limited understanding of the mechanism of the electrodeposition lead. It is mainly due to the complexity of the nucleation and growth process. Sheila M. Wong and Luísa M. Abrantes [13] studied Pb nucleation type from very alkaline media, while B.Scharifker and G.Hills [14] reported a 3D growth with instantaneous nucleation of lead electrodeposition in aqueous KNO_3. Pb overpotention-deposited

(OPD) with 3D progressive nucleation on *n*-Si(111) has been reported by Rashkova et al [2]. Moreover, Ehlers et al. [3] studied the influence of surface states on the kinetics of the initial stages of Pb electrodeposition on *n*-Ge (111).

Electrode surfaces modified with lead underpotential-deposited (UPD) monolayer exhibited unique and interesting structures and properties that were absent in the unmodified bare surfaces. In particular, UPD monolayer of Pb on various substrates was confirmed to catalyze the oxidation actions of formic acid [15-17], methyl alcohol and the reduction actions of peroxide reduction [18], oxygen [19, 20]. Pb UPD monolayer also had a considerable effect on the inhibition of hydrogen reduction reaction. Ion adsorption had significant influences on Pb UPD. The UPD of Pb on Cu(100) and Cu(111) in a chloride-containing electrolyte was accompanied by Cl^- desorption according to Brisard et al [21, 22]. Recent years, UPD from ionic liquid also were a hot topic.

Spectroscopic ellipsometry techniques offered the opportunity of characterizing the metal electrodeposition systems such as Cu/Au and Pb/Ag. SE is a nondestructive, sensitive measurement and do not require any sample preparation, which can sensitively monitor the gradual change of the surface films with 0.1 ~ 0.01 nm thickness and be used to obtain an accurate determination of surface film and bulk materials optical and dielectric properties such as refractive index, extinction coefficient or dielectric function under in/ex situ condition [23-26]. SE is based on measuring the change of polarization upon reflection or transmission from a material structure. The change in polarization ρ is traditionally expressed complex reflectance ratio in terms of

$$\rho = R_p / R_s = \tan\Psi e^{i\Delta} \quad (1)$$

where 'R_p'and 'R_s' are the amplitude reflection coefficients. Thus, '$\tan\Psi$' is the amplitude ratio upon reflection and 'Δ' is the phase shift.

In-situ ellipsometry has been successfully applied to bismuth telluride deposition on polycrystalline gold electrode by Zimmer et al [27]. Wu and coworkers [28] used oblique incidence reflectivity difference (OI-RD) as a probe, revealed differences of Pb OPD on polycrystalline Cu and on polycrystalline Au surfaces in the presence and absence of halide. Yet, the characterization and morphological real-time evolution of the Pb UPD layer had not been reported.

Here in, the real-time evolution of the Pb UPD layer on Cu was studied by monitoring optical responses of the electrode surface using spectroscopic ellipsometry. The optical data were fitted by introducing an effective medium approximation (EMA) model to obtain the volume fractions of Pb for different polarization potentials. The changing of current efficiency and optical constants of Pb UPD process were revealed.

2. EXPERIMENTAL

2.1. Materials and sample preparation

The substrate material for the specimens used in this work is polycrystalline copper. All the specimens were fabricated into disc-shaped electrode with 1 cm in diameter, and then embedded in epoxy resin leaving a working area of 0.785 cm^2. Prior to test, the electrode was subsequently ground

with 120 grit, 600 grit, 800 grit and 1200 grit emery papers, and ultrasonic cleaned in ultrapure water and ethanol for 5 min. The base-solution was 1 mmol/L $Pb(NO_3)_2$ + 100 mmol/L KNO_3, made from analytic grade reagents and ultrapure water (18.2 MΩ cm in resistivity). Prior to experiments, the solutions were deaerated by bubbling high-purity nitrogen through the solution. All tests were conducted at room temperature.

2.2. Electrochemical measurements

In order to perform the spectroscopic ellipsometry and electrochemical test simultaneously, a self-designed three-electrode cell was used, which is made of polytetrafluoroethylene, and the transmittance window is made of optical glass with high transmission coefficient. Electrochemical measurements were performed using a CHI600B electrochemical workstation (Shanghai Chenhua, China), where the disc-shaped copper was used as working electrode, a platinum foil as counter electrode, and a saturated calomel electrode (SCE) as reference electrode.

2.3. In-situ spectroscopic ellipsometry analysis

The spectroscopic ellipsometry of copper/solution interface during electrodeposition was measured by Woollam ellipsometer M-2000F. The electrolytic cell skeleton was made of Polytetrafluoroethylene (PTFE). Translucent windows were made of optical glass with high light transmission factors. The electrochemical cell was specially designed to monitor the optical responses of the working electrode during the electrochemical measurements. The measured wavelength range was from 400 nm to 800 nm with the incident angle of 70° (Fig. 1).

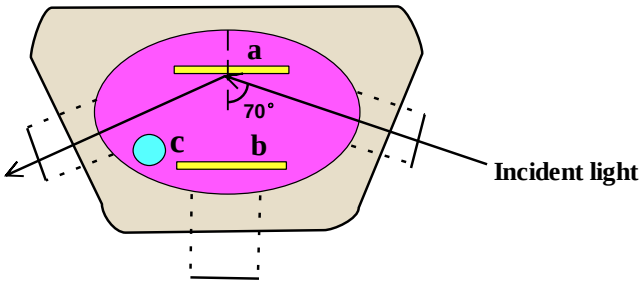

Figure 1. Electrolytic cell structure. (a) working electrode; (b) counter electrode; (c) reference electrode

3. RESULTS AND DISCUSSION

3.1. Cyclic voltammetry study

Figure 2 showed the cyclic voltammogram for Cu electrode measured in a solution containing 100 mmol/L KNO_3 with and without 1 mmol/L $Pb(NO_3)_2$. The potential was cyclically swept from

–200 mV to –600 mV. The dotted line showed cathodic current at the end of the scan potential, which corresponded to hydrogen reduction reaction on Cu electrode. By the addition of 1mmol/L Pb^{2+} in solution of 100 mmol/L KNO_3, the full line cyclic voltammogram was observed. Both the cathodic and anodic branches of the full line showed two current peaks, cathodic C1-C2 and anodic A1-A2. Labeled C1 is seen during the cathodic scan around −350 mV, corresponding to Pb UPD, while bulk deposition commences at –500 mV. Peaks corresponding to bulk and UPD Pb dissolution, labeled A1 around –300 mV and A2 around –450 mV.

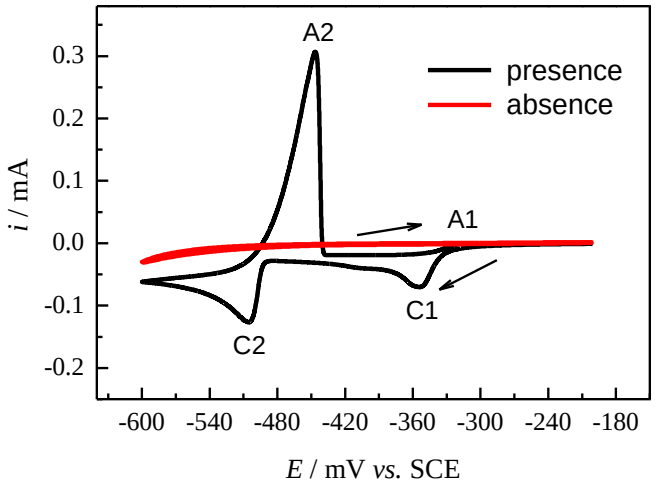

Figure 2. Cyclic voltammograms for Cu measured in 100 mmol/L KNO_3 solution in the absence of Pb^{2+} and in the presence of 1 mmol/L $Pb(NO_3)_2$. The scanning rate was 2 mV/s.

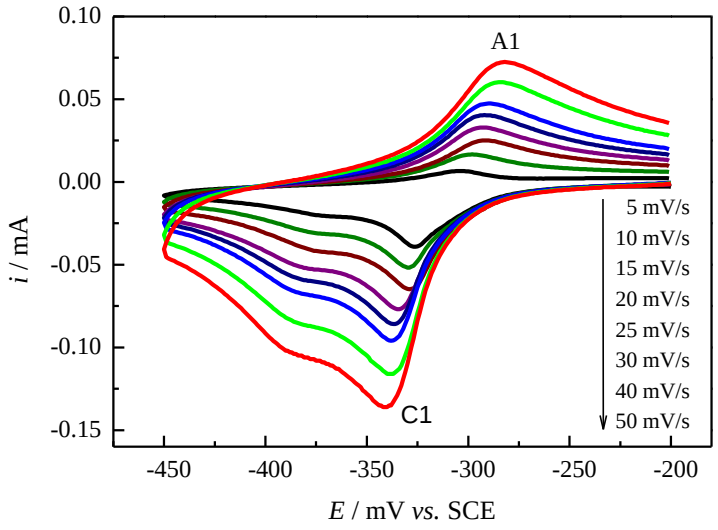

Figure 3. Cyclic voltammograms for Cu measured in 1 mmol/L $Pb(NO_3)_2$ and 100 mmol/L KNO_3 solution at different scanning rates.

CV responses for Cu measured in 1 mmol/L $Pb(NO_3)_2$ + 100 mmol/L KNO_3 solution at different scan rates, *v*, range from 5 to 50 mV/s were shown in Fig. 3. The negative potential was

limited at −450 mV to prevent the appearance of UPD Pb dissolution. The dates pointed to a quasi-reversible system because of the anodic to cathodic current peaks ratio, i_{pa}/i_{pc}, obtained at several sweep rates were lower than unity; the difference between anodic and cathodic potential peaks, $\Delta E_p = E_{pa} - E_{pc}$, were higher than 29.5 mV (2.3RT/nF).

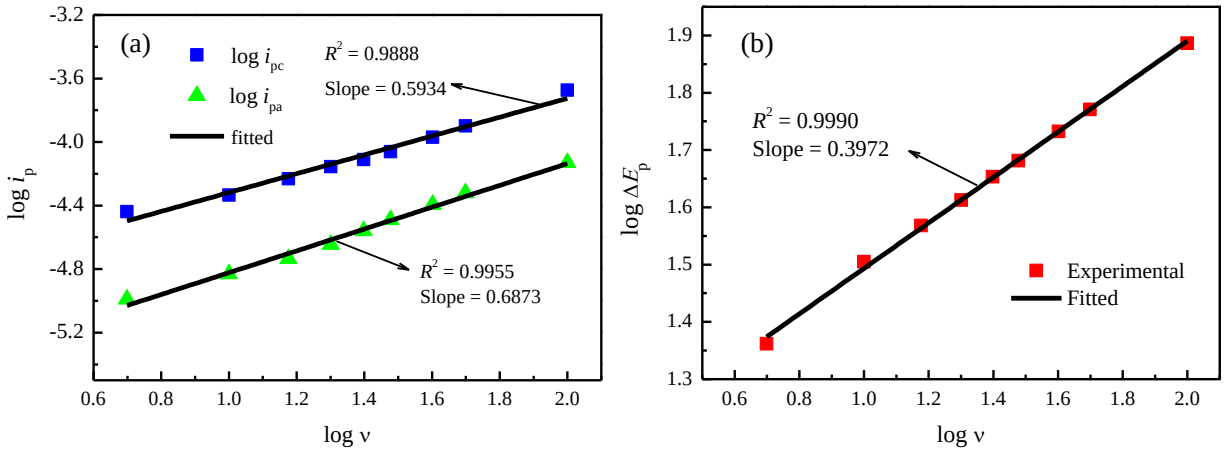

Figure 4. The analysis of cyclic voltammograms of Cu measured in 1 mmol/L $Pb(NO_3)_2$ and 100 mmol/L KNO_3 mixed solution obtained at different scanning rates: (a) log i_p *vs* log v; (b) log ΔE_p *vs* log v

Figure 4 showed the scan rate analysis of Pb UPD on Cu. It was seen that logi_{pc}, logi_{pa}, and logΔE_p were all linearly dependent on log$v$, and the slopes were 0.5934, 0.6873 and 0.3972, respectively. The results obeyed the analytical criteria for 2D phase change transitions of Sanchez-Maestre model [29] and we then concluded that Pb UPD occurs on Cu substrate was a two-dimensional nucleation and growth process.

3.2. Spectroscopic ellipsometry study

It has been acknowledged that for reflected light, this change in polarization, ρ, is often described with two values, Ψ and Δ, where Ψ is the ratio of reflected amplitudes and Δ is the phase difference produced upon reflection [30]. Fig. 5 showed obviously that the variety of Ψ became obviously rising and descending in the corresponding CV at the potential of the peak current orientation, and the variety rate of Δ was obvious, that was there were peaks while at the peak current. Extreme changes also proved that Ψ and Δ changes were corresponding to the electrochemical reaction of the electrode system, and it could reflect Pb UPD and Pb OPD on Cu substrate. So it demonstrated that spectroscopic ellipsometry was feasible method to characterize the electro-deposition process of Pb. The emergence of the extreme showed that the changes of Ψ and Δ value reflected the interface characteristic variation of the electrode system. After one cycling, Ψ and Δ values went back to the initial value. It indicated that the UPD reaction system was a quasi-reversible process and was consistent with the cyclic voltammetry measured in Fig. 3.

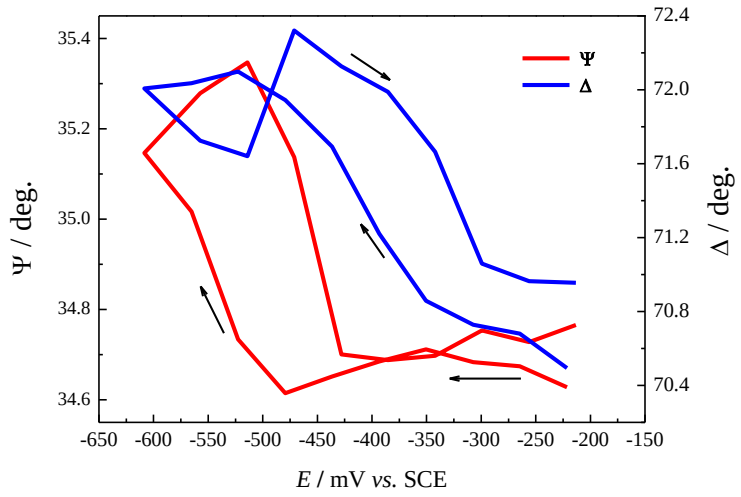

Figure 5. Experimental ellipsometric parameter Ψ and Δ simultaneously recorded during the potential scan

3.2.1. Optical model

Pb UPD has proven to be 2D phase change process. Here we assumed that Pb UPD was monolayer. The remaining gaps were filled with solution. The physical model of Pb UPD was shown in Fig. 6a. Optical model shown in Fig. 6b was described as the ambient solution-mixed layer-copper substrate.

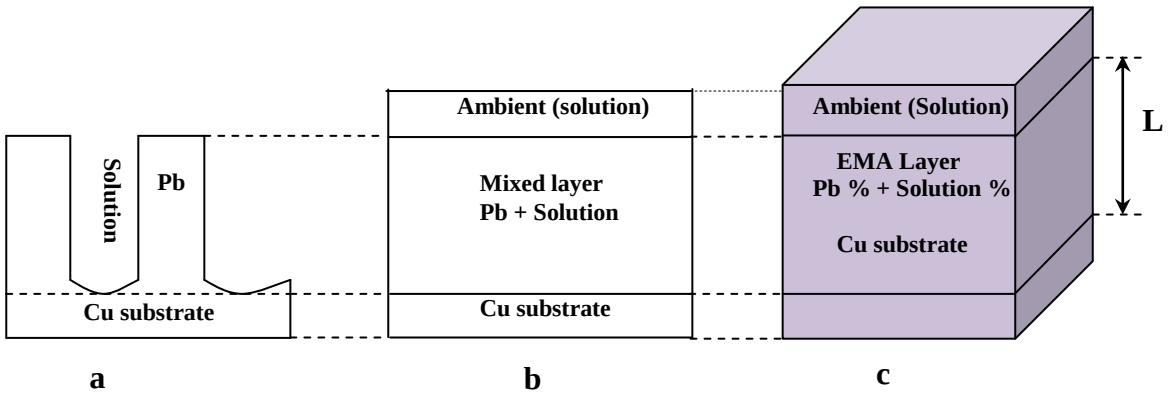

Figure 6. Physical model (a) optical model (b) and EMA model (c) of Pb UPD on polystalline Cu used for spectroscopic ellipsometry spectra interpretation.

The optical data were fitted by introducing the effective medium approximation (EMA) model (Fig. 6c). Each layer was described by its thickness and optical constants. In this model, the thickness of EMA layer was assumed to be 4.6 Å (Pb monatomic diameter), the volume fraction of Pb and solution were fitted. The parameters of the model were determined by minimizing the mean square error (MSE) defined as equation (2):

$$\mathrm{MSE} = \frac{1}{n-1}\sum_{i=1}^{n}\left[\left(\Psi_i^c - \Psi_i^e\right)^2 + \left(\Delta_i^c - \Delta_i^e\right)\right] \qquad (2)$$

where '*c*' stands for the calculated and '*e*' stands for the experimental, *n* is the number of experimental points. In the fittings, a Marquard method was used to minimize the MSE [27].

3.2.2. Fitting results

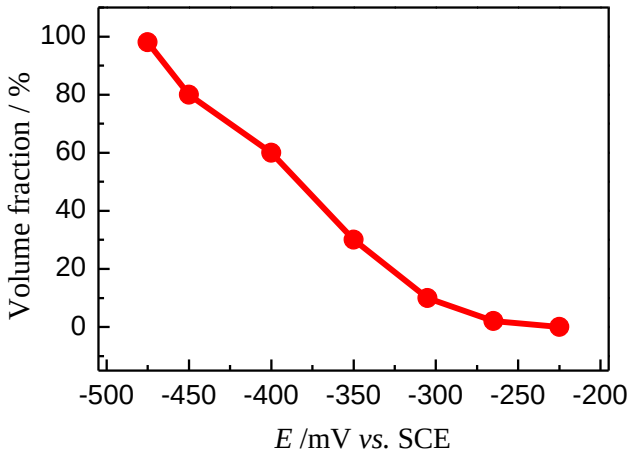

Figure 7. Volume fraction variation of Pb during the cathodic cyclic voltammetry process

Figure 7 showed the volume fraction variation of Pb with cathodic scan potential. The curve showed the evolution of the fitted from EMA model. Noted that the developing trends of curve was on the rise, and the slope increased significantly, which shown that as the potential turned negative, the total deposition of Pb increased, and the increasing rate went upward. It also has been found that Pb volume fractions were less than 100%. This meant that Pb UPD layer was monatomic and the volume fraction could be viewed as the UPD coverage. Therefore, during –200 mV ~ –480 mV, the coverage of Pb UPD increased and the increasing rate went up. We also can concluded that the assuming of a 100% current efficiency was not well-formed, the causes lay in the fact that non-ignorable double layer charge and hydrogen reduction reaction (shown as Fig. 2).

Vladislavic and co-workers analysised the experimental current transients, obtained with glassy carbon electrode and graphite electrode, revealed that increment Bi^{3+} concentration changes nucleation mechanism from three-dimensional (3D) progressive nucleation toward instantaneous. It illustrated the change of current can responsed reaction process [31]. In this study, we explained the electroplating process by using current efficiency test. Figure 8 gave the evolution of the current efficiency during Pb UPD. At the onset of Pb UPD, the current efficiency was close to zero. Subsequently, the current efficiency increased to its maximum at −350 mV and then it dropped at more negative potentials. Pb UPD phenomenon can be formulated as following:

$$\mathrm{Cu} + \mathrm{Pb}^{2+} + 2e^- \leftrightarrow \left(\mathrm{CuPb}\right)_{\mathrm{UPD}};\ E_{\mathrm{Cu/Pb}} \qquad (3)$$

where $E_{\mathrm{Cu/Pb}}$ is the reversible Pb UPD potential, and it might be estimated from the mean of the anodic voltametric current peaks (C1) and cathodic voltametric current peaks (A1) in Fig. 2. It was

clear that the initial polarization potential was more positive, consequently nearly all current was used for the double layer charge. When the polarization potential was close to −350mV, Pb^{2+} might gain electrons from Cu substrate surface and Pb^{2+} began reduction, this resulted the increasing current efficiency. But, after the electrode potential exceeded −350 mV, Pb^{2+} consumption made Pb^{2+} concentration near Cu substrate surface decreased while the residue electric charges rose, and the current efficiency was then falling off.

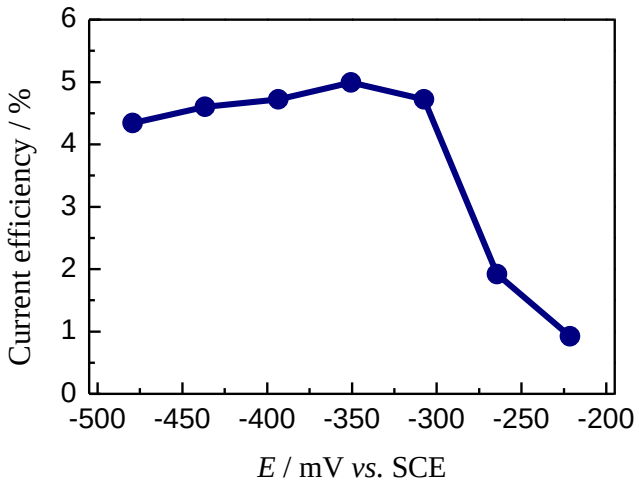

Figure 8. Current efficiency of Pb UPD during the cathodic cyclic voltammetry process

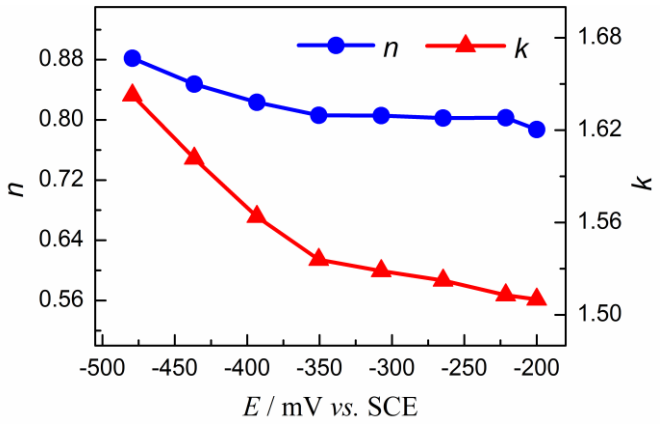

Figure 9. Optical constants vs. polarization potential at λ=545nm. Fitted values of optical constants were obtained from spectroscopic ellisometric measurements using EMA model (see in Fig.6c).

At the same way, Figure 9 showed the change of the optical constants, while EMA layer was observed from −200 to −350 mV, n and k were in tiny change, which indicated that only a small amount of lead was deposited at this potential and the lead coverage on copper substrate is low. Subsequently, the values of the optical constants caused increasing clearly from −350 to −500 mV, respected that UPD Pb layer formed constantly. Above all the reversible Pb UPD potential is −350mV.

The extinction index has the similar trend as refraction index with increasing of the potentials of electrodepositited Pb layer. Therefore, in situ SE is able to provide kinetics of lead electrodeposition [32].

4. CONCLUSIONS

This work demonstrated that a two dimensional nucleation and growth process was observed for UPD of Pb on polycrystalline Cu using both in situ SE and CV. Fitting results showed that double layer charge and hydrogen reduction reaction cannot be ignored. The current efficiency first increased, and then decreased. When polarization potential equaled to −350 mV, the current efficiency reached maximum.

ACKNOWLEDGEMENTS
This work was supported by Natural Science Foundation of China (No. 21376282), and Chongqing Innovation Fund for Graduate Students (No. CYB14019).

Reference

1. D. Pavlov, *J Power Sources* 46 (1993) 171.
2. B. Rashkova, B. Guel, R.T. Potzschke, G. Staikov, W.J. Lorenz, *Electrochim Acta* 43 (1998) 3021.
3. C. Ehlers, U. Konig, G. Staikov, J.W. Schultze, *Electrochim Acta* 47 (2001) 379.
4. L.H. Mascaro, E.K. Kaibara, L.O. Bulhoes, *J Electrochem Soc* 144 (1997) L273.
5. L.O.S. Bulhoes, L.H. Mascaro, *J Solid State Electr* 8 (2004) 238.
6. C.O. Avellaneda, M.A. Napolitano, E.K. Kaibara, L.O.S. Bulhoes, *Electrochim Acta* 50 (2005) 1317.
7. E. Gyenge, J. Jung, B. Mahato, *J Power Sources* 113 (2003) 388.
8. R. Bertoncello, S. Cattarin, I. Frateur, M. Musiani, *J Electroanal Chem* 492 (2000) 145.
9. Y.A. Ivanova, D.K. Ivanou, E.A. Streltsov, *Electrochim Acta* 53 (2008) 5051.
10. T.M. Garakani, P. Norouzi, M. Hamzehloo, M.R. Ganjali, *Int J Electrochem Sci* 7 (2012) 857.
11. F. Xiao, B. Yoo, M.A. Ryan, K.H. Lee, N.V. Myung, *Electrochim Acta* 52 (2006) 1101.
12. B. Sun, Z.T. Yang, X.W. Zou, Z.Z. Jin, *Mater Chem and Phys* 86 (2004) 144.
13. S.M. Wong, L.M. Abrantes, *Electrochim Acta* 51 (2005) 619.
14. B. Scharifker, G. Hills, *Electrochim Acta* 28 (1983) 879.
15. M.J. Zhang, C.P. Wilde, *J Electroanal Chem* 390 (1995) 59.
16. S.Y. Uhm, S.T. Chung, J.Y. Lee, *Electrochem Commun* 9 (2007) 2027.
17. L. Guo, J.H. Tan, W.P. Li, G. Hu, S.T. Zhang, *Prog Chem* 25 (2013) 1842.
18. S.J. Hsieh, A.A. Gewirth, *Surf Sci* 498 (2002) 147.
19. I. Oh, A.A. Gewirth, J. Kwak, *J Catal* 213 (2003) 17.
20. S.A.S. Machado, A.A. Tanaka, E.R. Gonzalez, *Electrochim Acta* 39 (1994) 2591.
21. G.M. Brisard, E. Zenati, H.A. Gasteiger, N.M. Markovic, P.N. Ross, *Langmuir* 11 (1995) 2221.
22. G.M. Brisard, E. Zenati, H.A. Gasteiger, N.M. Markovic, P.N. Ross, *Langmuir* 13 (1997) 2390.
23. S.H. Yang, Y. Liu, Y.L. Zhang, D. Mo, *Surf Interface Anal* 41 (2009) 502.
24. T. Byrne, L. Lohstreter, M.J. Filiaggi, Z. Bai, J.R. Dahn, *Surf Sci* 602 (2008) 2927.
25. T.A. Mykhaylyk, N.L. Dmitruk, S.D. Evans, I.W. Hamley, J.R. Henderson, *Surf Interface Anal* 39 (2007) 575.

26. K. Vedam, *Thin Solid Films* 313 (1998) 1.
27. A. Zimmer, N. Stein, L. Johann, R. Beck, C. Boulanger, *Electrochim Acta* 52 (2007) 4760.
28. G.Y. Wu, S.E. Bae, A.A. Gewirth, J. Gray, X.D. Zhu, T.P. Moffat, W. Schwarzacher, *Surf Sci* 601 (2007) 1886.
29. M.S. Maestre, R. Rodriguezamaro, E. Munoz, J.J. Ruiz, L. Camacho, *J Electroanal Chem* 373 (1994) 31.
30. G.E. Jellison, F.A. Modine, *Appl Phys Lett* 69 (1996) 371.
31. N. Vladislavic, S. Brinic, Z. Grubac, M. Buzuk, *Int J Electrochem Sci* 9 (2014) 6020.
32. W.P. Li, S.T. Zhang, *Appl Surf Sci* 257 (2011) 3275.